Magneto-Mechanical Model of Passive Magnetic Axial Bearings versus the Eccentricity Error, Part II: Application and Results

Roberto Muscia

Department of Engineering and Architecture
University of Trieste, Trieste, Italy
muscia@units.it

Abstract — In this paper we apply the physical mathematical model described in Part I [1]. The study shows: i) the influence of the eccentricity of two polarized rings of the bearing on the stiffness; ii) the numerical efficiency of the response surfaces for evaluating the magnetic field in any point of the domain fixed; iii), in relation to a demanding application example (possible replacement of a big axial oleodynamic bearing with a thrust magnetic passive bearing), the danger arising from possible resonances (the natural frequencies of the device are near to the excitation frequencies).

Index Terms — Levitation, magnetic bearings, magnetostatic field, natural frequencies, stiffnesses.

I. INTRODUCTION

With reference to the formulations illustrated in Part I, some numerical computations to evaluate forces/ moments, stiffnesses, and natural frequencies relative to an application example have been performed. The calculation of the magnetic induction was executed first thing. This computation is based on the response surfaces [2]. The components $B_x(\mathbf{P}')$, $B_y(\mathbf{P}')$, and $B_z(\mathbf{P}')$ have been evaluated in a certain number of points suitably arranged on the surface where we compute $\mathbf{B}(\mathbf{P}')$. Subsequently, a surface that interpolates the values of $B_x(\mathbf{P}')$, $B_y(\mathbf{P}')$, and $B_z(\mathbf{P}')$ is defined. The two dimensional domain of the surface is represented by the integration parameters that define the polar coordinates of the generic point $\mathbf{P}'$ (in general these coordinates are r and θ). In Fig. 1, an example of response surface is illustrated. For example, the points $\mathbf{P}'$ where $B_x(\mathbf{P}')$ is computed are indicated by a small circle. In this way we can virtually have infinite points $\mathbf{P}'$ where the magnetic induction is known without performing other integrations: as soon as we fix r and θ we can immediately interpolate the corresponding value of $\mathbf{B}(\mathbf{P}')$. The interpolation is so fast that it is possible to perform the integration to compute forces and moments in a few seconds. Moreover, as illustrated in Fig. 1, by plotting $B_x(r,\theta)$, $B_y(r,\theta)$, and $B_y(r,\theta)$ a check of the interpolation fitness can be easily performed: the response surface must not show anomalous peaks, it has to be a continuous function of r and θ. All these computations have been performed by using *Mathematica* [3]. These computations can surely be performed by using the finite elements methods [4], [5] but, the computing time can be much longer. In relation to the influence of the inclination angle α of the magnetization **M** (see Fig. 2 in Part I [1]), we observe that it has always a constant value. Consequently, the quantity $\sin\alpha$ has always been put out from all the integral signs defined in Part I [1] for computing the magnetic inductions, forces and moments. This fact enables us to compute at once the previous quantities relative to each angle α lower than 90 degrees as soon as the same quantities have been computed with $\alpha = 90$ degrees. As a matter of fact, to perform the magnetic inductions computation, we have only to multiply each value obtained with $\alpha = 90$ degrees by the sine of the new angle $\alpha < 90$ degrees. In the case of forces, moments, and stiffnesses, the values evaluated with $\alpha = 90$ degrees have to be multiplied for the square of the sine of the new angle $\alpha < 90$ degrees.

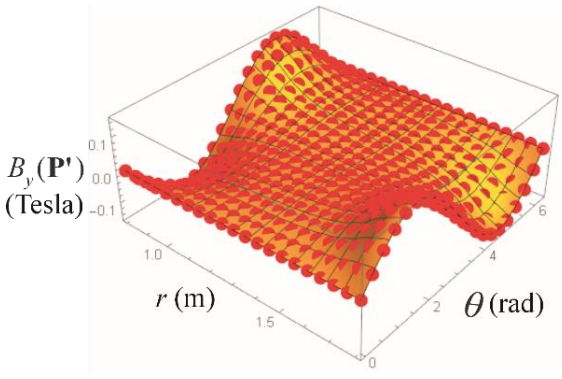

Fig. 1. Response surface for magnetic induction computation relative to 441 points (r,θ).

Submitted On: October 15, 2016
Accepted On: March 23, 2017

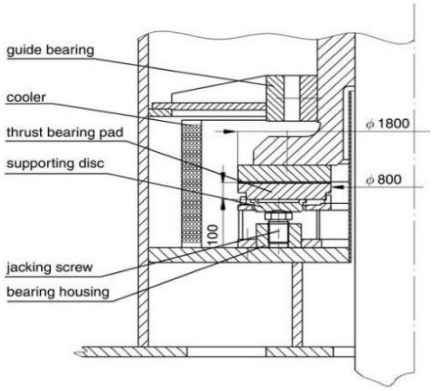

Fig. 2. Some real dimensions of a hydrounit thrust bearing with Kaplan turbine [8].

II. A DEMANDING APPLICATION EXAMPLE

The physical mathematical model previously described in Part I [1] has been applied to define a possible initial step in dimensioning of a thrust magnetic passive bearing. This bearing should be able to generate the same thrust of a big axial oleodynamic bearing assembled in a hydrounit for electrical generation. With reference to an axial passive magnetic bearing that can generate a thrust equal about to 30 KN, some researchers [6], [7] are experimentally testing such kind of solution. In relation to a real hydrounit for electrical generation, in Fig. 2 [8] the inner and outer diameters of the relative oleodynamic bearing are reported in mm. Figure 3 [8] shows the thrust bearing pads of the bearing. The positioning of the bearing is indicated in Fig. 9 in Part I [1] (see the particular C) and the axial dimension of the bearing pads is equal to 100 mm (see Fig. 2). Over the bearing pads, the upper ring integral to the vertical shaft has a thickness also equal about to 100 mm. Unlike the bearing pads, the upper ring rotates together with the shaft. Therefore, in relation to our application example, for the polarized rings illustrated in Fig. 1 in Part I [1] we can fix the following dimensions: h=100 mm, r_i=400 mm, and r_e=900 mm. The bearing pads and the upper ring would be substituted by the polarized rings A and B, respectively. Polarized rings of the previous size could be practically manufactured by superimposing many smaller polarized angular sectors. The thrust that the hydrodynamic bearing generates during a stationary working is very high and is equal to 5.5×10^6 N (with a rotational speed equal to 187.5 rpm). In order to obtain magnetic levitation forces so high, it is necessary to fix a very high value of the magnetization vector **M**. Nowadays, with reference to available neodymium magnets, the maximum value of the corresponding module $|\mathbf{M}|$ is equal to 11.38×10^5 A/m [9]. However, as we will discuss in the following Section III, also if we use this high value of $|\mathbf{M}|$, by considering an air gap ranging from 20 to 30 mm, we obtain about one-fifteenth of the thrust generated by the hydrodynamic bearing illustrated in Figs. 2 and 3. Therefore, in order to achieve the above-mentioned thrust by passive magnetic levitation, it would be necessary to utilize at least sixteen polarized rings B (see Fig. 2 in Part I [1]) integral to the shaft and sixteen rings A integral to the base. From an engineering point of view, this number of rings is certainly too high. However, if we consider a Halbach configuration [10] of each polarized ring as illustrated in Fig. 4 [11], we could reduce the number of the rings magnets in such a way that a feasibility study could be considered. With reference to our demanding application example, since a Halbach magnets configuration could increase the attractive force of about fifty percent, assuming that the increase is true also when the facing magnets that generate repulsive forces, we could utilize only eight pairs of polarized rings. With reference to this configuration we observe that eight rings A (see Fig. 1 in Part I [1]) have to be fixed to the non-rotating frame. The other eight rings B will be fixed to the shaft of the rotor-generator system. For example, four pairs A, B of rings could be arranged to define the upper axial bearing (see the area C in Fig. 9 in Part I [1]). The other four pairs of polarized rings A, B could be put under the rotor. Consequently, the axial height of each upper and lower magnetic passive bearing would be a bit greater than (100+100+20)x4=880 mm [20 mm represents a mean air gap t between each pair of rings and 100 mm is h (see Fig. 1 in Part I [1])]. The values of the air gap have been fixed from a possible engineering point of view in relation to a hypothetic stationary working condition of the device. The natural angular frequencies $\omega_{em_{tot}}$ and $\omega_{tm_{tot}}$ were evaluated with reference to Eqs. (25) and (26) in Part I [1], respectively, by considering the total mass m_{tot} equal to 5.775×10^5 Kg plus 31200 Kg of 16 polarized rings: m_{tot} = 6.087×10^5 Kg. The value of 5.775×10^5 Kg is greater than 5% with respect to the value of 5.5×10^5 Kg. The 5.5×10^5 Kg has been simply obtained by computing the mass that corresponds to the load of 5.5×10^6 N due to the gravity acceleration. This load is applied to the oleodynamic bearing. Moreover, in order to compute the frequencies ω_{em_i} and $\omega_{em_{tot}}$ by Eqs. (24) and (25) in Part I [1], respectively, in relation to all the simplifications considered, we can also assume,

$$m_1 + m_2 + m_3 + m_4 = m_{tot}. \quad (1)$$

Consequently, we obtain:

$$\omega_e = \omega_{em_h} = \omega_{em_{tot}}, \quad (2)$$

$$\omega_t = \omega_{tm_h} = \omega_{tm_{tot}}. \quad (3)$$

Moreover, if we consider eight pairs of polarized rings with eight Halbach rings B keyed on the shaft and

eight Halbach rings A fixed to the base of the structure, the stiffnesses K_t and K_e relative to each pair of rings A, B non Halbach must be multiplied by 16 (the magnetic "springs" work in a parallel way). Consequently, the new equations for computing ω_e and ω_t relative to the two uncoupled vertical and horizontal DOFs (Degrees of Freedom) are the following [see Eqs. (22), (23), (25), and (27) in Part I]:

$$K_{tze}(t) = \frac{\partial F_z(t)}{\partial t}, \tag{4}$$

$$\omega_{tze}(t) = \sqrt{\frac{16K_{tze}(t)}{m_{tot}}}, \tag{5}$$

$$K_{ezt}(e) = \frac{\partial F_z(e)}{\partial e}, \tag{6}$$

$$\omega_{ezt}(e) = \sqrt{\frac{16K_{ezt}(e)}{m_{tot}}}, \tag{7}$$

$$K_{eyt}(e) = \frac{\partial F_y(e)}{\partial e}, \tag{8}$$

$$\omega_{eyt}(e) = \sqrt{\frac{16K_{eyt}(e)}{m_{tot}}}. \tag{9}$$

The maximum value of the eccentricity e considered in the numerical simulations was put equal to 0.01 m. However, in relation to a correct working of the hydrounit, e=0.01 m certainly is not an acceptable value (it is too high). Maximum values of e about equal or lower than 0.0001 m should be considered. Nevertheless, from the simulation point of view, the previous maximum value e=0.01 m has been fixed to test the fitness of the modelization. In this respect, we observe that the forces, stiffnesses, and natural angular frequencies must be always continuous functions of e. Always in order to check the correctness of the model, the air gap t range has been fixed from 0.003 m to 0.5000 m. From a possible practical point of view, when the device works under a stationary condition, the real value of t could reasonably change from 0.01 to 0.05 m.

Fig. 3. Tilting-pads thrust bearing [8].

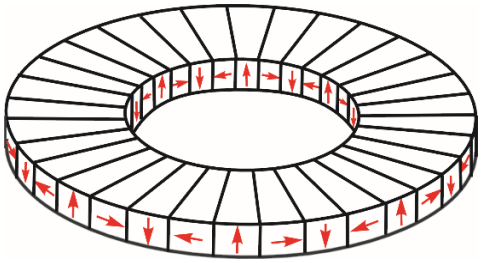

Fig. 4. A Halbach configuration [10] of a polarized ring [11].

III. RESULTS

The results that have been obtained versus the air gap t and the eccentricity e are: i) the magnetic induction **B** on the ring horizontal surfaces of the upper magnet; ii) the levitation force; iii) the axial and radial stiffnesses of the bearing; iv) the natural frequencies in correspondence with certain values of the mass m_{tot}. Table 1 summarizes the main data utilized to perform some simulations. The computation of the magnetic induction was executed in the points $\mathbf{P}_1'$ and $\mathbf{P}_2'$ of the upper and lower surfaces, respectively, of the polarized ring B. 441 points on each surfaces have been fixed. The polar coordinates of these points are defined by a radius r and an angle θ (see Fig. 6 in Part I [1]). The values of r and the correspondent angle θ have been fixed by the following relations:

$$r = r_i + \frac{(r_e - r_i)}{k_r} i, \tag{10}$$

$$\theta = \frac{2\pi}{k_\theta} j, \tag{11}$$

where i=0, 1, …, k_r and j=0, 1, …, k_θ. This kind of discretization of the surfaces allows us to obtain good response surfaces and limit the computation time to few tens of seconds (by using a computer with an Intel I5 and 4 GB of RAM). An example of these results is illustrated in the previously cited Fig. 1. Another example concerning the magnetization induction vectors relative to the upper surface of the ring B with t=0.050 m, e=0.000 m, and α=90 degrees is illustrated in Fig. 5. We observe the complete axial symmetry of the field. The same symmetry characterizes all the magnetic field configurations computed by using any value of the eccentricity e and α (see Table 1). This fact confirms that the law of energy conservation is respected because such a symmetry implies that the moment τ_z around the axis Z [see Eq. (20) in Part I [1]] is always equal to zero. As a matter of fact, the numerical evaluations performed have always given values of τ_z almost equal to zero or relatively small. In this regard, we observe that the component F_x of the resultant force **F** applied to the polarized ring B should be equal to zero. Therefore, it

is sufficient that the difference between F_{x1} and F_{x2} (components of the forces applied to the lower and upper surfaces of the ring B, $F_x = F_{x1}+F_{x2}$) is equal to a few newtons and τ_z at once reaches a value higher than zero, for example 3 Nm. Nevertheless, in relation to the precision of the numerical simulations, it is necessary to consider the orders of magnitude of the quantities evaluated. In the case study we observe that F_z and also F_y (when e is greater than zero) are equal to hundred thousands of newtons. Moreover, overall they were computed by a kind of formulation similar to that used to evaluate F_x. Therefore, with reference to the approximations that affect the numerical integration in the study context, we can consider the numerical results obtained for F_x and τ_z very good, i.e., a good approximation of zero. In this respect, a typical trend of F_x versus $0.003 \le t \le 0.015$ m (with e=0 and α=90 degrees) is illustrated in Fig. 6. When different values of the parameter e is fixed, similar trends have been obtained. In relation to the values obtained for F_z versus the air gap t, Fig. 7 shows some curves examples. The curves have been achieved by fixing α=90, 70, and 30 degrees, eccentricity e=0.000 m and the values of t reported in Table 1. With reference to a non-operative working condition of the magnetic bearing for the hydrounit application example, we also have performed some calculations with an air gap t=0.003 m. In order to assure a non-dangerous working condition of the system, this value is certainly too small. This air gap could be easily set to zero as a consequence of a small axial overload together with planarity, perpendicularity, etc. errors. In this case, to avoid the destruction of the device, mechanical "catcher" bearings could be suitably integrated around and outside the rings of the magnetic bearings. In Fig. 8 the axial stiffnesses $K_{tze}(t)$ corresponding to the previous F_z (see Fig. 7) are reported. These stiffnesses have been evaluated by Eq. (4). Figure 9 shows the relative angular natural frequencies $\omega_{tze}(t)$ computed by Eq. (5). In Fig. 10 a comparison among three functions $F_z(e)$ is presented. Three values of the air gap t have been considered: t= 0.003, 0.010, 0.020 m. We note that the vertical levitation force changes enough versus the value of t. In relation to the scale of the representation of the graphs, as soon as t is fixed, it could seem that $F_z(e)$ is almost independent of e. Nevertheless, by using Eq. (6) we note that the axial stiffness $K_{ezt}(e)$ shows significantly different trends versus the three values of t (see Fig. 11). If, by Eq. (7) we compute the correspondent axial natural angular frequency $\omega_{ezt}(e)$, we obtain the various resonance conditions of the system along the vertical DOF versus the correspondent values of the eccentricity e. Figure 12 shows $\omega_{ezt}(e)$: it can change from about 2 to 24 rpm. With reference to the component F_y applied to the polarized ring B, in Fig. 13 the corresponding trend versus e is reported. The curves are relative to the three values of air gap t previously considered. We note that the radial force F_y is sufficiently independent of t and increases almost linearly versus e. By deriving $F_y(e)$ with respect to e, we obtain the radial stiffness K_{eyt} of the levitation system [see Eq. (8)]. Figure 14 shows the functions $K_{eyt}(e)$ versus t. By observing these curves, the nonlinearity of $F_y(e)$ is pointed out. By using Eq. (9) we obtain the corresponding radial natural angular frequencies $\omega_{eyt}(e)$. These frequencies vary from about 64.5 to 68.7 rpm (see Fig. 15). As noted in Section I, the values of forces and stiffnesses relative to an angle α of inclination of the magnetization **M** lower than 90 degrees, can be simply obtained by multiplying the corresponding values computed with α=90 degrees by $\sin^2\alpha$. For the corresponding natural angular frequency the multiplicative factor is equal to $\sin\alpha$. Consequently, when α decreases, also the stiffnesses and natural frequencies become lower.

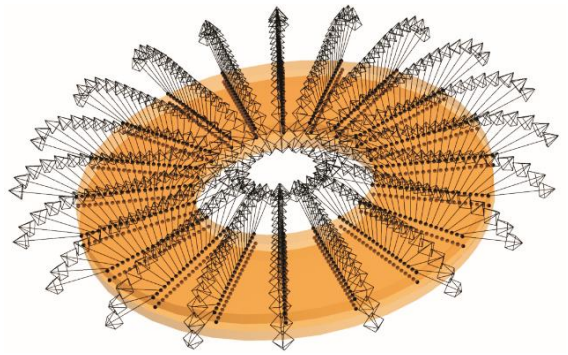

Fig. 5. Magnetization induction vectors in 441 points of the upper surface of the upper polarized ring B (see Fig. 1 in Part I).

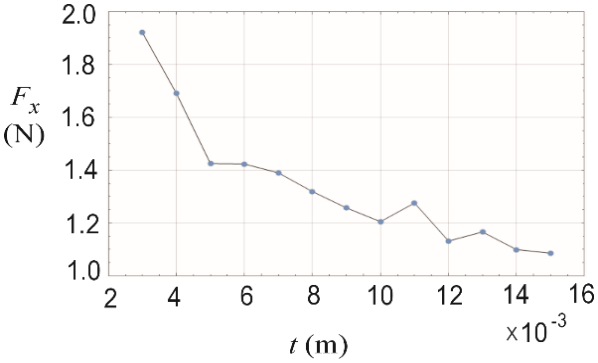

Fig. 6. A typical trend of the radial force F_x when e=0 and α=90 degrees versus the air gap t.

Table 1: Parameters used for the numerical simulations

Module of the Uniform Magnetization $\|\mathbf{M}\|$	11.38×10^5 A/m
Inner radius of the magnets r_i	0.4 m
Outer radius of the magnets r_e	0.9 m
Free space permeability μ_0	$4\pi\times10^{-7}$ Wb/Am
α	90, 70, 30 degrees
e	0.000, 0.001, 0.002, …, 0.010 m
t	0.003, 0.004, …, 0.012, 0.015, 0.017, 0.020, 0.025, 0.030, 0.035, 0.040, 0.050, 0.075, 0.100, 0.150, 0.200, 0.300, 0.400, 0.500 m
h	0.1 m
m_{tot}	6.087×10^5 Kg
Number k_r of subdivision intervals of r_e-r_i	20
Number k_θ of subdivision intervals of 2π	20
Number $(k_r+1)\times(k_\theta+1)$ of points where the magnetic induction has been computed	441

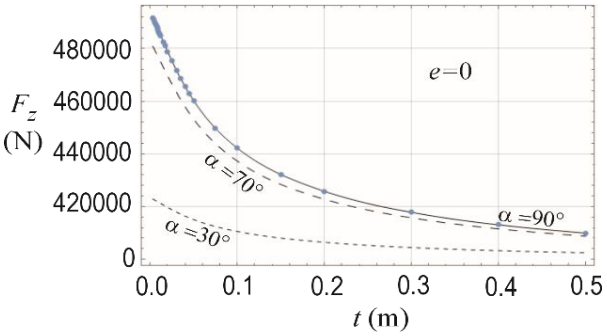

Fig. 7. Vertical levitation force F_z when e=0 versus the air gap t and the angle α.

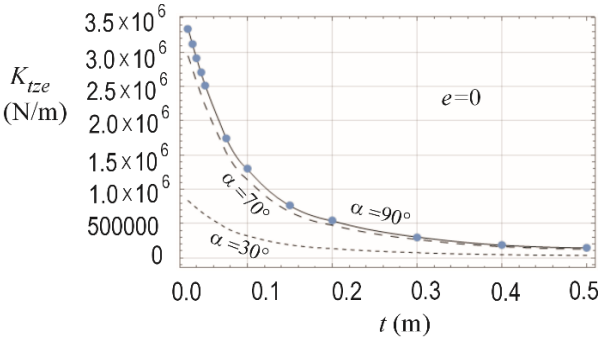

Fig. 8. Stiffnesses K_{tze} versus the air gap t when e=0 versus the air gap t and the angle α.

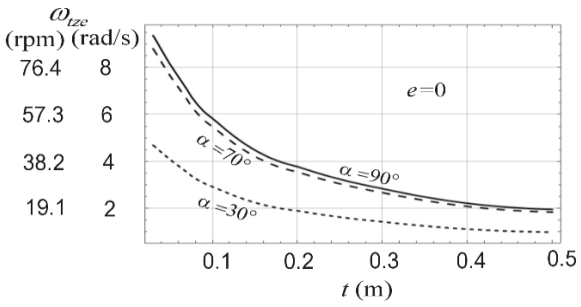

Fig. 9. Axial angular natural frequency ω_{tze} versus the air gap t and the angle α when the eccentricity e=0.

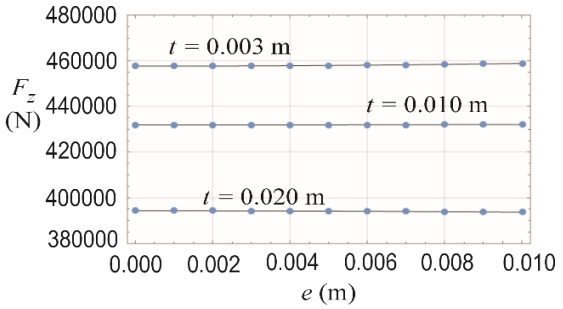

Fig. 10. Interpolation of the force F_z relative to three air gap values t versus the eccentricity e, with α=90 degrees.

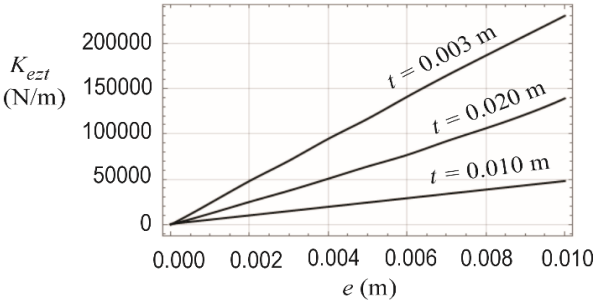

Fig. 11. Axial stiffness K_{ezt} relative to three air gap t values versus the eccentricity e, with α=90 degrees.

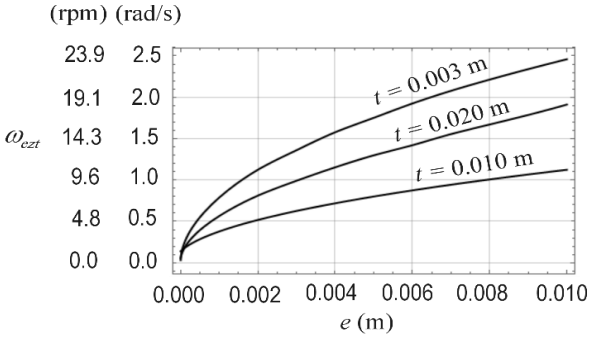

Fig. 12. Axial angular natural frequency ω_{ezt} relative to three air gap t values versus the eccentricity e, with α=90 degrees.

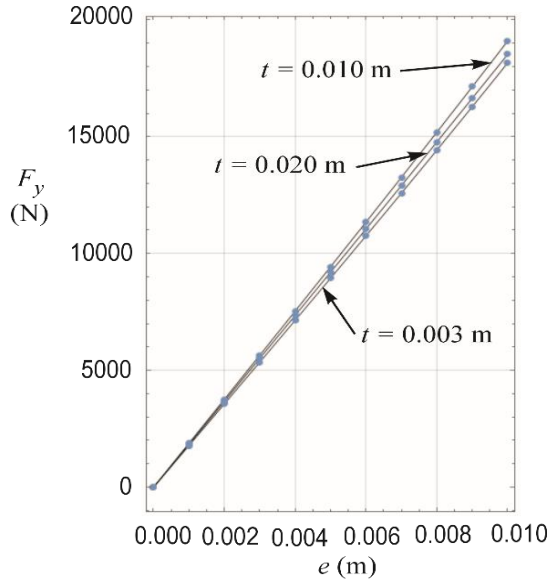

Fig. 13. Force F_y relative to three air gap values t versus the eccentricity e, with α=90 degrees.

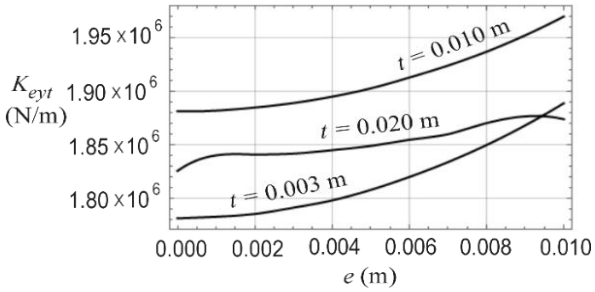

Fig. 14. Radial stiffness K_{eyt} relative to three air gap t values versus the eccentricity e, with α=90 degrees.

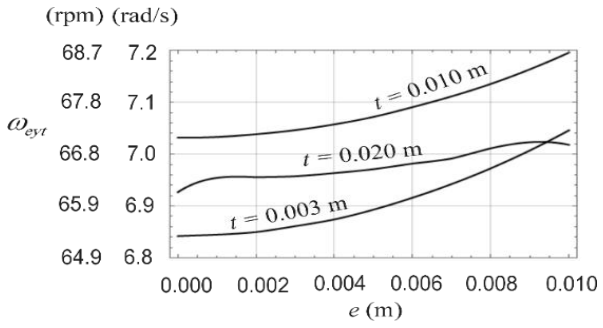

Fig. 15. Radial angular natural frequency ω_{eyt} relative to three air gap t values versus the eccentricity e, with α=90 degrees.

IV. SOME CONSIDERATIONS ON THE RESULTS OBTAINED

With reference to the vertical levitation force we note that in the domain $0.000 \leq e \leq 0.010$ m F_z varies very little (see Fig. 10). Conversely, the corresponding curve of $F_y(e)$ shows an almost linear variation, from 0 to about 20000 N (see Fig. 13). The component F_x (e), in general is several orders of magnitude lower than $F_y(e)$ and, overall, $F_z(e)$. As previously mentioned, F_x (e) should be equal to zero, whatever the value of e is. The irregular trend of $F_x(e)$ depends on the number of effective digits fixed to perform the integrations. In this respect, we note that all the integrations have been performed by setting a precision for the computation with five effective digits of accuracy [3]. If a greater number of effective digits is fixed (for example 15), the computation time becomes very high and, in general, significant improvements of the results are not obtained (only small differences affect the results achieved with 5 and 15 effective digits). From an engineering point of view, we observe that a high value of stiffness (axial and radial) as much as possible independent of the air gap and the eccentricity would be suitable. In the case of the passive magnetic levitation this condition is partially met. Moreover, the angular natural frequencies are lower than the stationary rotation speed of the hydrounit (187.5 rpm). Therefore, during periods of start-ups and shutdowns the system passes more or less quickly through its resonant frequencies. If this passage is not quite fast, dangerous vibrations can arise. With reference to the simplified model illustrated in Fig. 8 (a) in Part I [1], we observe that it can reflect reality better than the one reported in Fig. 8 (b), also in Part I. However, the lateral instability of the magnetic levitation [12] is also confirmed by observing the trend of the force F_y (see Fig. 13): it quickly increases versus the eccentricity. Finally, we observe that in spite of the simplifications, the results obtained and the relative considerations suggest which basic problems can arise if we consider substituting a classic hydrodynamic thrust bearing with passive magnetic bearings. We can note that also the hydrodynamic bearings have their drawbacks [13]. Therefore, possible preliminary studies of alternative solutions could be acceptable.

V. CONCLUSION

The knowledge of the natural vibration frequencies of a system is important to avoid an operating condition where the frequencies of the excitation forces are near or equal to the above-mentioned natural frequencies. The passive bearings are parts of a mechanical system and determine the corresponding natural frequencies versus the applied load and the oscillating masses. In order to avoid dangerous resonances or beats it is convenient to evaluate how these frequencies change in function of different operating conditions. In the case study it was found that a reduction of the air gap beyond certain limits causes a significant increase of the stiffness of the axial bearing. Consequently, we obtain an increase of the natural frequency of the system. Therefore, the larger the load applied the higher the aforesaid frequency. This

behavior is similar to that which was found in another study concerning the passive radial bearings [14]. With reference to the demanding application example, this fact can surely be advantageous if we were able to increase the natural frequencies to a speed higher than the stationary rotational speed of the device (187.5 rpm). Unfortunately, higher natural frequencies correspond to too small air gaps that, from an engineering point of view, cannot be accepted. This problem could be studied and, perhaps, solved, by considering additional permanent magnets. The position of these magnets should be controlled by a feedback system versus the instantaneous values of air gaps and natural frequencies. Finally, if we consider a nonlinear magnetization **M** of the ring magnets, the details of the mathematical model illustrated in Part I [1] enable a very fast and easy modification to compute the field and the forces due to the surface charge density $\sigma_M(\mathbf{P})$.

REFERENCES

[1] R. Muscia, "Magneto-mechanical model of passive magnetic axial bearings versus the eccentricity error, Part I: Physical mathematical model," *ACES Journal*, 2017.

[2] G. E. P. Box and D. Norman, *Response Surfaces, Mixtures, and Ridge Analyses*, Second edition, Wiley, 2007.

[3] *Mathematica* 10.3 (2016), http://www.wolfram.com/mathematica

[4] S. Wu, S. Zuo, X. Wu, F. Lin, and J. Shen, "Magnet modification to reduce pulsating torque for axial flux permanent magnet synchronous machines," *ACES Journal*, vol. 31, no. 3, pp. 294-303, March 2016.

[5] Y. Chen and K. Zhang, "Electromagnetic force calculation of conductor plate double Halbach permanent magnet electrodynamic suspension," *ACES Journal*, vol. 29, no. 11, pp. 916-922, November 2014.

[6] J. J. Pérez-Loya, C. J. D. Abrahamsson, F. Evestedt, and U. Lundin, "Initial performance tests of a permanent magnet thrust bearing for a hydropower synchronous generator test-rig," *AIM2016*, Bormio, Italy, March 14-16, 2016.

[7] J. J. Pérez-Loya, J. De Santiago, and U. Lundin, "Construction of a permanent magnet thrust bearing for a hydropower generator test setup," *1st Brazilian Workshop on Magnetic Bearings – BWMB*, Rio de Janeiro, Brazil, October 2013.

[8] L. Dabrowski and M. Wasilczuk, "Evaluation of water turbine hydrodynamic thrust bearing performance on the basis of thermoelastohydrodynamic calculations and operational data," *Proceedings of the Institution of Mechanical Engineers, Part J: Journal of Engineering Tribology*, vol. 218, pp. 413-421, 2004.

[9] Neodymium Magnets-An Expert Information Source, E-magnets, UK, Northbridge Road, Berkhamsted, Hertfordshire, HP4 1EH, 2016. http://www.ndfeb-info.com

[10] K. Halbach, "Design of permanent multipole magnets with oriented rare earth cobalt material," *Nucl. Instrum. Methods*, vol. 169, pp. 1-10, 1981.

[11] D. J. Eichenberg, C. A. Gallo, and W. K. Thompson, "Development and Testing of an Axial Halbach Magnetic Bearing," Report *NASA Center for Aerospace Information*, Hanover, MD 21076–1320, 2006.

[12] R. J. Duffin, "Free suspension and Earnshow's theorem," *Archive for Rational Mechanics and Analysis*, vol. 14, iss. 1, pp. 261-263, January, 1963.

[13] M. Wasilczuk, "Friction and lubrication of large tilting-pad thrust bearings," *Lubricants*, vol. 3, pp. 164-180, 2015.

[14] L. Zidarič, "Studio delle Configurazioni di Equilibrio di Cuscinetti Magnetici Passivi," *Dissertation* (in Italian), University of Trieste, Department of Engineering and Architecture, Trieste, Italy, 2012.

Supplementary Materials

For further information concerning the *Mathematica* programming, you can contact the author at muscia@units.it.

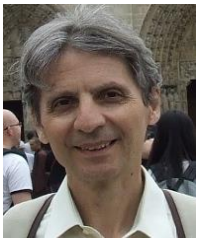

Roberto Muscia Professor at the University of Trieste, Trieste, Italy. He received his Master's degree in Mechanical Engineering from the University of Trieste in 1981. From 1983 to 1998 he was Researcher with the same university. From 1998 he is Associate Professor. At the present time his research interests focus on the study of mechanical problems in magnetic devices to improve their design.